JOURNAL OF THERMOPHYSICS AND HEAT TRANSFER
Vol. 8, No. 4, Oct.–Dec. 1994

Thermal Analysis of an Arc-Heater Electrode with a Rotating Arc Foot

Frank S. Milos*
NASA Ames Research Center, Moffett Field, California 94035
and
Charles E. Shepard†
Eloret Institute, Palo Alto, California 94303

Analytic formulations are presented for the analysis of an arc-heater electrode with a rotating arc foot. Two limiting cases, a smoothly rotating arc foot and an arc foot that jumps between multiple sticking points, are analyzed. For each case the temperature distribution for a copper electrode is obtained for the plausible range of operating conditions. It is shown that the smoothly rotating arc foot is an extremely safe mode of operation, whereas the jumping arc foot produces excessively high electrode surface temperatures. It is suggested to eliminate arc-foot rotation and rely on a distribution of fixed electrodes with stationary arc attachment to avoid electrode failure at high current.

Nomenclature

d = coefficient defined by Eq. (5), 1/cm
f = rotational frequency, Hz
i = imaginary unit: $i^2 = -1$
k = thermal conductivity, W/cm-K
N = number of sticking points
Q = maximum heat flux, W/cm^2
q = heat flux at inner electrode surface, W/cm^2
R = electrode radius, cm
R_s = arc-foot radius, cm
T = temperature, K
t = time, s
x = circumferential coordinate, cm
y = inward radial coordinate, cm
z = rotating circumferential coordinate, cm
α = thermal diffusivity, cm^2/s
δ = electrode wall thickness, cm
δ_{ij} = Kronecker delta
θ = circumferential angle, rad
λ = coefficient defined by Eq. (15), 1/s
τ = heat pulse duration, s
Φ = dimensionless hot-wall temperature
ω = angular frequency, $2\pi f$, rad/s

Subscripts
c = cold wall
m = radial Fourier series index
n = circumferential Fourier series index
0 = zero term for Fourier series

Superscript
s = steady solution for stationary arc foot

Introduction

CONSTRICTED, electric arcjets have been used for almost 30 yr to produce high enthalpy gases for materials testing and for simulation of hypersonic flight heating conditions.[1,2] To reduce impurity levels in the test stream and to enhance the lifetime of electrodes, magnetically driven electrodes were developed.[3] In these electrodes, the operating current passes through internal coils to create a toroidal magnetic field that exerts a circumferental Lorentz force on the arc foot, thereby causing the arc foot to rotate around the circumference of the ring-shaped electrode. The most successful application of this technology to date is in the Interaction Heating Facility (IHF) at NASA Ames, which operates up to 6400 A and 60 MW with a package of 16 magnetically driven electrodes (8 upstream anodes and 8 downstream cathodes).[4]

A significant operational cost and annoyance is electrode replacement, which occurs on average in about 10^4 A-h for an IHF electrode. Electrode wear patterns[3,5] and high-speed films[6–8] suggest that for magnetically driven electrodes, different modes of arc-foot attachment and movement can occur. Figure 1 illustrates several possible modes of arc-foot rotation in order of increasing local thermal severity. In all cases the magnetic field is inducing a net clockwise rotation of the arc foot. The most benign mode of operation is the smoothly rotating arc foot that distributes the heat flux uniformly around the circumference of the electrode. The most severe mode of operation is the jumping arc foot, where the arc foot repeatedly visits certain spots on the electrode surface. These spots suffer severe heating, and a hole can be melted through the electrode. The number of sticking points ($N = 3$ in the illustration) is not known. This jumping mode is possible be-

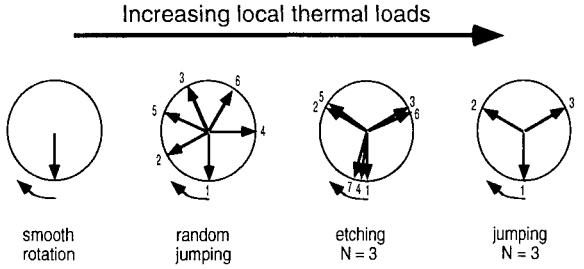

Fig. 1 Possible arc foot rotation modes in a magnetically-driven electrode. The net rotation rate is ©(100) Hz in the clockwise direction.

Presented as Paper 93-2855 at the AIAA 28th Thermophysics Conference, Orlando, FL, July 6–9, 1993; received Sept. 13, 1993; revision received March 7, 1994; accepted for publication April 11, 1994.

*Aerospace Engineer, Thermal Protection Materials Branch. Member AIAA.
†Research Scientist, Thermosciences Institute. Member AIAA.

cause the arc may prefer to attach on a location that has been preheated, or which lacks an oxide coating, owing to a previous visitation by the arc foot. The random-jumping mode is probably not detrimental to electrode lifetime, provided the arc foot does not remain too long on any given location and does not prefer to revisit any specific location. In the etching mode of operation, the arc foot attaches on spots adjacent to previously visited locations. This mode, which is akin to adding a precession to the jumping arc foot, could be responsible for the common "grooved" pattern of electrode wear.[3]

Unfortunately, there is no reliable theory for predicting under what conditions or how frequently the different modes of arc-foot movement will occur, but there is evidence that arcs become more unstable as the current density is increased.[6-8] There also is high uncertainty in the details of arc-foot attachment, such as the variation of spot size and net rotation rate with flowfield and operating conditions. Nevertheless, future arc-heater designs call for higher current in the electrodes to produce higher test-stream enthalpy.[9] Since the nonsteady modes of arc-foot rotation may not be preventable, heat transfer in the different modes of operation must be considered as part of the electrode-design process. Therefore, in this work we present a simplified analysis of the electrode heat transfer for the two limiting cases from Fig. 1: 1) the smoothly rotating arc foot and 2) the jumping arc foot. Dimensional results are presented for IHF operating conditions, and nondimensional results are presented for a plausible range of operating parameters for existing and possible future electrode designs.

Background Information

An IHF arc-heater electrode receives heat flux from internal electrical resistance, from the flowfield, and from arc-foot heating. The internal resistance heating depends on the electrode design and on the current level, is typically well below 10 kW, and is distributed in some manner within the electrode. The aerodynamic heating is of $\mathcal{O}(100)$ kW per electrode, is distributed at $\mathcal{O}(1)$ kW/cm^2 over the inner surface of the electrode, and produces a background temperature rise of under 100 K in the electrode. The heating at the arc foot owing to cathode fall potential is 10–20 kW in normal operation, but is highly concentrated with peak heat flux estimated[3,7] to be of $\mathcal{O}(100)$ kW/cm^2.

Electrode failure occurs if the high heat flux at the arc foot cannot be dissipated by local cooling mechanisms without raising the surface temperature significantly above the melting point (1356 K for copper). In normal, high-current operation, the electrode surface will have a very thin melt film and a small vaporization rate. We observe electrode mass loss of about 1 mm in 4–10 h of operation. Using 5000 J/g as the energy to melt and then to vaporize copper and a spot size of 1 mm, heat rejection owing to mass removal is well below 0.5 kW/cm^2. Heat loss by reradiation is also below 0.4 kW/cm^2 at the vaporization temperature of copper (2868 K). Since both of these values are negligible compared with the peak heating, we are justified in performing a conduction-only analysis for dissipation of the high local heat flux at the arc foot. For a prescribed arc-foot heat flux, we will require the maximum temperature not to significantly exceed the melting point, because such a condition would indicate melting of a significant thickness of the electrode wall.

The nominal geometric and operating parameters for this electrode study, based on conditions in the IHF, are presented in Table 1. Because the electrode wall thickness is small relative to the electrode radius ($\delta/R < 0.05$), curvature effects will be neglected in the analysis. The arc-foot parameters are tabulated in order of decreasing certainty. Total arc-foot heating ranges from 10 to 20 kW in normal operation (25 V and 400–800 A per electrode), but higher current-carrying capability is desired for future designs. The arc-foot rotation rate is not well known. Reported values[3,5,8,10] for magnetically driven electrodes fall in the range of 100–500 Hz. The arc radius has not been measured. Erosion patterns[3] from IHF electrodes suggest spot sizes of $\mathcal{O}(1)$ mm for operation below 10 atm, but it is not clear whether these erosion patterns arise from normal or abnormal arc-foot attachment and rotation. If the jumping mode of arc-foot rotation occurs, the number of jumping points is probably a small integer, but it may be possible to design an electrode configuration that forces the arc to jump among 6–8 predetermined locations. The peak heat flux is estimated to range from 75 to 300 kW/cm^2. Since it is unlikely that copper can function as a high current cathode without the existence of melt, it can be postulated that in stable operation the arc-foot radius becomes at least small enough to create a thin melt layer on the surface. A copper anode, in contrast, can operate without a melt layer.

Analysis

This section contains analysis of the conduction heat transfer in the electrode owing to rotation of the arc foot. Figure 2 presents a cross section of the electrode geometry and the coordinate system. The electrode is in essence a large, thin-walled ring. The exterior surface is water cooled, and the interior surface is heated by the moving arc foot. The aerodynamic heating is low compared with the heating at the arc foot. The lateral faces of the electrode are insulated; in reality the electrode may consist of a number of electrode segments that are insulated from each other. We use a two-dimensional model for the electrode heat transfer and constant thermal properties. The latter assumption is reasonable for oxygen-free copper in the temperature range of interest. With the assumption of constant properties, the heat conduction equation is linear and amenable to mathematical analysis. The electrode wall is thin compared with electrode radius; therefore, we neglect curvature in the radial direction and use a local coordinate y that points inward from the cooled surface. On the heated surface the heat flux $q(\theta, t)$ is prescribed. The cooling water never boils in normal operation, but we conservatively estimate the exterior-surface temperature as T_c = 373 K to account for the temperature rise owing to the background aerodynamic heating. A convective heating condition can be used at the cooled surface; however, this boundary condition greatly complicates the numerical procedures and introduces an additional independent dimensionless parameter. The convective boundary condition will be treated in a separate paper.

Smoothly Rotating Arc Foot

For this case, we assume that the arc foot rotates steadily with frequency $\omega = 2\pi f$ around the circumference of the inner

Table 1 Electrode and arc-foot parameters

Parameter	Nominal range or value
R	6.0 cm
δ	0.254 cm
$\pi R_s^2 Q$	10–20 kW
f	100–500 Hz
R_s	0.05–0.5 cm
N	2–8
Q	75–300 kW/cm^2

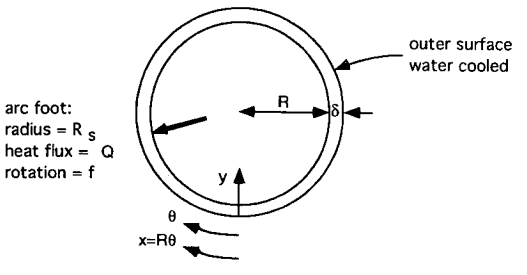

Fig. 2 Two-dimensional electrode geometry and coordinate system.

electrode surface. With this assumption, the heat flux at the inner surface can be written $q(z)$, where $z = R(\theta - \omega t)$. In the rotating coordinate frame and neglecting curvature, the equation for transient heat conduction becomes

$$\frac{\partial^2 T}{\partial z^2} + \frac{\partial^2 T}{\partial y^2} = \frac{1}{\alpha}\left(\frac{\partial T}{\partial t} + R\omega \frac{\partial T}{\partial z}\right) \tag{1}$$

where $T = T(z, y, t)$, with boundary conditions

$$\begin{aligned} T &= T_c \quad \text{at} \quad y = 0 \\ k\frac{\partial T}{\partial y} &= q(z) \quad \text{at} \quad y = \delta \end{aligned} \tag{2}$$

We seek the quasisteady solution ($\partial T/\partial t = 0$) that is obtained after many rotations of the arc foot. The solution has periodicity $2\pi R$ in the z direction; therefore, with no loss of generality, the temperature and heat flux can be represented as complex Fourier series

$$\begin{aligned} T(z, y) &= \sum_{n=-\infty}^{\infty} T_n(y) e^{inz/R} \\ q(z) &= \sum_{n=-\infty}^{\infty} q_n e^{inz/R} \end{aligned} \tag{3}$$

where

$$\begin{aligned} q_n &= \frac{1}{2\pi R}\int_{-\pi R}^{\pi R} q(z) e^{-inz/R}\, dz \\ T_n(y) &= \frac{1}{2\pi R}\int_{-\pi R}^{\pi R} T(z, y) e^{-inz/R}\, dz \end{aligned} \tag{4}$$

Substitution into Eq. (1) shows that

$$T_n'' = \left(\frac{n^2}{R^2} + i\frac{n\omega}{\alpha}\right) T_n = d_n^2 T_n \tag{5}$$

and, by application of the boundary conditions

$$T(z, y) = T_c + \frac{yq_0}{k} + \sum_{n=-\infty}^{\infty}{}' \frac{q_n \sinh d_n y}{k d_n \cosh d_n \delta} e^{inz/R} \tag{6}$$

where the sum excludes the $n = 0$ term. The solution is real (not complex) for any real function q, because the $\pm n$ terms are complex conjugates. The peak temperature occurs somewhere on the heated surface, where

$$T(z, \delta) = T_c + \frac{\delta q_0}{k} + \sum_{n=-\infty}^{\infty}{}' \frac{q_n \tanh d_n \delta}{k d_n} e^{inz/R} \tag{7}$$

Any function can be used for the heat flux. In particular, the simple square-wave heat flux

$$q(z) = \begin{cases} Q, & |z| < R_s \\ 0, & |z| \geq R_s \end{cases} \tag{8}$$

where R_s has Fourier coefficients

$$\begin{aligned} q_0 &= \frac{QR_s}{\pi R} \\ q_n &= \frac{Q}{n\pi} \sin \frac{nR_s}{R} \end{aligned} \tag{9}$$

For the square-wave heat flux, the inner wall temperature in dimensionless form can be written

$$\begin{aligned} \Phi &= \frac{k\pi[T(z, \delta) - T_c]}{2QR_s} \\ &= \frac{\delta}{2R}\left(1 + \frac{R}{R_s}\sum_{n=-\infty}^{\infty}{}' \frac{\tanh \delta d_n}{n\delta d_n} \sin \frac{nR_s}{R} e^{inz/R}\right) \end{aligned} \tag{10}$$

The left side scales the temperature rise with $2QR_s/k\pi$. The right side is a function of the independent variable z/R and of the dimensionless quantities $\delta^2\omega/\alpha$, δ/R, and R_s/R. Equation (10) is easily evaluated numerically using complex functions, provided that branch cuts are carefully taken into account.

Jumping Arc Foot

For this case, we assume that the arc foot sticks at N points distributed in some manner around the circumference of the inner electrode surface, the arc remains stationary on each successive sticking point for $1/Nf$ seconds, and the arc-foot heat flux has a symmetric profile. The latter assumption allows the use of cosine Fourier series. For example, for a sticking point centered at $\theta = 0$

$$q(x) = \sum_{n=0}^{\infty} q_n \cos \frac{nx}{R}$$

where

$$\begin{aligned} q_0 &= \frac{1}{2\pi R}\int_{-\pi R}^{\pi R} q(x)\, dx \\ q_n &= \frac{1}{\pi R}\int_{-\pi R}^{\pi R} q(x) \cos \frac{nx}{R}\, dx \end{aligned} \tag{11}$$

where $x = R\theta$. The square-wave heat flux has Fourier coefficients

$$\begin{aligned} q_0 &= \frac{QR_s}{\pi R} \\ q_n &= \frac{2Q}{n\pi} \sin \frac{nR_s}{R} \end{aligned} \tag{12}$$

The solution for this case is constructed by superposition of several problems. We continue with analyses of a sticking point centered at $\theta = 0$. The steady solution for continuous heating [$\nabla^2 T = 0$, Eq. (2), and Eq. (11)] by inspection can be written

$$T = T_c + T^s$$

where

$$T^s = \frac{yq_0}{k} + \frac{R}{k}\sum_{n=1}^{\infty} \frac{q_n \cos\left(\frac{nx}{R}\right) \sinh\left(\frac{ny}{R}\right)}{n \cosh\left(\frac{n\delta}{R}\right)} \tag{13}$$

The transient solution for heating that begins at $t = 0$ is Eq. (13) minus an unsteady part that contains a double Fourier series expansion of T^s

$$T = T_c + T^s - \sum_{n=0}^{\infty}\sum_{m=0}^{\infty} T^s_{nm} \cos \frac{nx}{R} \sin \frac{(2m+1)\pi y}{2\delta} e^{-\lambda_{nm} t} \tag{14}$$

where

$$\frac{\delta^2\lambda_{nm}}{\alpha} = \left(\frac{n\delta}{R}\right)^2 + \left[\frac{(2m+1)\pi}{2}\right]^2$$
$$T^s_{nm} = \frac{(-1)^m 2\alpha q_n}{k\delta\lambda_{nm}} \tag{15}$$

Note that $T = T_c$ at $t = 0$, and $T \to T_c + T^s$ as $t \to \infty$. When the heating pulse is turned off ($t \geq 1/Nf$), the solution becomes a sum of exponentially decaying terms:

$$T = T_c + \sum_{n=0}^{\infty}\sum_{m=0}^{\infty} T^s_{nm} \cos\frac{nx}{R} \sin\frac{(2m+1)\pi y}{2\delta} \times (1 - e^{-\lambda_{nm}/Nf}) e^{-\lambda_{nm}(t-1/Nf)} \tag{16}$$

The transient solution after many heating pulses is obtained by summing the solution for the current pulse from Eq. (15) or (16) with the decaying solutions for all previous pulses from Eq. (16). The pulses are separated by time $1/f$. For $t \geq 1/Nf$ the repetitive-pulse solution is Eq. (16) with the last exponential term multiplied by

$$(1 + e^{-\lambda_{nm}/f} + e^{-2\lambda_{nm}/f} + \cdots)$$

Since this quantity equals

$$(1 - e^{-\lambda_{nm}/f})^{-1}$$

the repetitive-pulse solution is

$$T = T_c + \sum_{n=0}^{\infty}\sum_{m=0}^{\infty} T^s_{nm} \cos\frac{nx}{R} \sin\frac{(2m+1)\pi y}{2\delta} \times \left(\frac{1 - e^{-\lambda_{nm}/Nf}}{1 - e^{-\lambda_{nm}/f}}\right) e^{-\lambda_{nm}(t-1/Nf)}, \qquad t \geq 1/Nf \tag{17}$$

For $t < 1/Nf$, the repetitive-pulse sum is obtained in a similar manner. The solution simplifies to

$$T = T_c + T^s - \sum_{n=0}^{\infty}\sum_{m=0}^{\infty} T^s_{nm} \cos\frac{nx}{R} \sin\frac{(2m+1)\pi y}{2\delta} \times \left[\frac{1 - e^{-\lambda_{nm}(1/f - 1/Nf)}}{1 - e^{-\lambda_{nm}/f}}\right] e^{-\lambda_{nm}t}, \qquad t < 1/Nf \tag{18}$$

The final step in the analysis is to add the influence of the heat flux at the N sticking locations. For each of the sticking points, either Eq. (17) or (18) applies (depending on the current location of the arc foot); however, the solutions must be shifted in time and space. For convenience, we now assume that the N sticking points are distributed uniformly around the circumference of the electrode. Owing to the symmetry of the problem, we need only to consider the time interval $0 < t \leq 1/Nf$ for a pulse centered at $x = 0$. The relevant solution is

$$T = T_c + T^s - \sum_{n=0}^{\infty}\sum_{m=0}^{\infty} T^s_{nm} \cos\frac{nx}{R} \sin\frac{(2m+1)\pi y}{2\delta} \times \left[\frac{1 - e^{-\lambda_{nm}(1/f - 1/Nf)}}{1 - e^{-\lambda_{nm}/f}}\right] e^{-\lambda_{nm}t} + \sum_{j=1}^{N-1}\sum_{n=0}^{\infty}\sum_{m=0}^{\infty} T^s_{nm} \times \cos\left[\frac{nx}{R} - (1 - \delta_{n0})\frac{2\pi j}{N}\right] \sin\frac{(2m+1)\pi y}{2\delta} \times \left(\frac{1 - e^{-\lambda_{nm}/Nf}}{1 - e^{-\lambda_{nm}/f}}\right) \exp\{-\lambda_{nm}[t + (j-1)/Nf]\} \tag{19}$$

where the triple sum accounts for the heat flux at the other sticking locations, and the Kronecker delta eliminates x dependence for the $n = 0$ terms.

We are primarily interested in the maximum electrode temperature, which occurs somewhere on the heated surface at the end of the heat pulse. From Eq. (19), and employing the double Fourier expansion for T^s, we have

$$T(x, \delta, 1/Nf) = T_c + \sum_{j=0}^{N-1}\sum_{n=0}^{\infty}\sum_{m=0}^{\infty} \frac{2\alpha q_n}{k\delta\lambda_{nm}} \times \cos\left[\frac{nx}{R} - (1 - \delta_{n0})\frac{2\pi j}{N}\right] \left(\frac{1 - e^{-\lambda_{nm}/Nf}}{1 - e^{-\lambda_{nm}/f}}\right) e^{-\lambda_{nm}j/Nf} \tag{20}$$

To evaluate Eq. (20), it is easiest to store λ_{nm}/Nf and the nm terms in the sum for $j = 0$. Then for each successive j, we multiply each term by $e^{-\lambda_{nm}/Nf}$ and rotate the solution by $\Delta x = 2\pi/N$. The coefficients λ_{nm} and T^s_{nm} are obtained from Eq. (15), and the temperature is given by Eq. (20), which can be recast in dimensionless form

$$\Phi = \frac{k\pi[T(x, \delta) - T_c]}{2QR_s} = \sum_{j=0}^{N-1}\sum_{n=0}^{\infty}\sum_{m=0}^{\infty} \frac{\pi\alpha q_n}{\delta R_s \lambda_{nm}} \times \cos\left[\frac{nx}{R} - (1 - \delta_{n0})\frac{2\pi j}{N}\right] \left(\frac{1 - e^{-\lambda_{nm}/Nf}}{1 - e^{-\lambda_{nm}/f}}\right) e^{-\lambda_{nm}j/Nf} \tag{21}$$

The right side is a function of x/R, $\delta^2\omega/\alpha$, δ/R, R_s/R, and N.

Results

This section presents both selected dimensional results and nondimensional results for parametric variations in the geometric and operating parameters. We begin with results for the smoothly rotating arc foot. Figure 3 presents dimensional results for the temperature of the heated surface [from Eq. (10)] for two values of Q and two values of f. The arc-foot radius is varied to maintain the same total heat flux (20 kW) for all four cases. This figure represents the maximum IHF cathode heating conditions. In this and subsequent figures the arc foot is moving toward the left and is currently centered at location $\theta = 0$.

As shown in Fig. 3, the effect of increasing rotation rate is to disperse the heat flux: the minimum temperature increases, and the maximum temperature is significantly reduced. At a

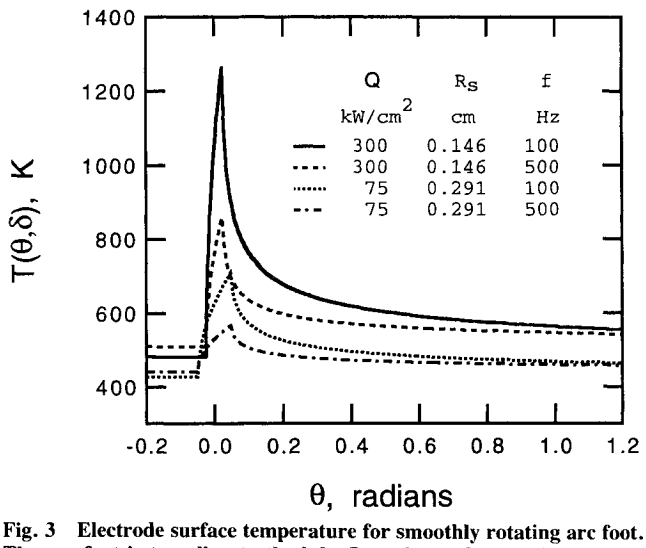

Fig. 3 Electrode surface temperature for smoothly rotating arc foot. The arc foot is traveling to the left. R = 6 cm, δ = 0.254 cm, and $\pi R_s^2 Q$ = 20 kW.

Table 2 Peak temperature for smoothly rotating arc foot

Q, kW/cm^2	$\pi R_s^2 Q$, kW	T_{max}, K 100 Hz	T_{max}, K 500 Hz
75	10	650	528
75	20	711	568
300	10	1125	772
300	20	1285	869

R and δ from Table 1.

Table 3 Φ_{max} for smoothly rotating arc foot with $\delta/R = 0.02$

$\delta^2\omega/\alpha$	R_s/R values 0.005	0.010	0.022	0.050	0.100	0.220
5	0.315	0.225	0.152	0.102	0.072	0.049
7	0.268	0.191	0.130	0.087	0.062	0.043
10	0.226	0.162	0.110	0.074	0.053	0.037
15	0.186	0.134	0.092	0.063	0.045	0.032
22	0.155	0.112	0.078	0.053	0.039	0.028
33	0.129	0.093	0.065	0.045	0.034	0.025
50	0.106	0.078	0.055	0.039	0.029	0.022
70	0.091	0.067	0.048	0.034	0.026	0.020
100	0.078	0.058	0.042	0.030	0.024	0.019
200	0.058	0.044	0.032	0.024	0.020	0.016

Table 4 Peak temperature for jumping arc foot with $Q = 75$ kW/cm^2

N	$\pi R_s^2 Q$, kW	T_{max}, K 100 Hz	T_{max}, K 500 Hz
2	10	2961	2617
2	20	3202	2862
3	10	2373	1990
3	20	2532	2153
5	10	1806	1450
5	20	1913	1548
8	10	1447	1121
8	20	1507	1182

R and δ from Table 1.

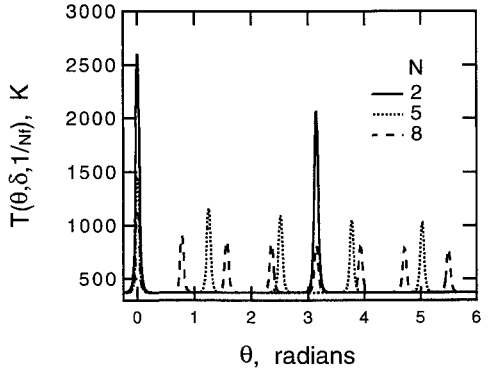

Fig. 4 Electrode surface temperature for jumping arc foot. $R = 6$ cm, $\delta = 0.254$ cm, $f = 500$ Hz, $Q = 75$ kW/cm^2, and $\pi R_s^2 Q = 10$ kW. The arc foot is currently located at $\Phi = 0$, but is about to jump to another location.

heat flux of 300 kW/cm^2, the peak temperature is reduced approximately 400 K by increasing the rotation rate from 100 to 500 Hz. The effect is less pronounced for the larger spot size. The surface is close to the melt temperature for the low frequency, small spot case. At the higher frequency, a small spot radius with heat flux above 300 kW/cm^2 would be required to bring the surface to the melting point.

The dimensional calculations were repeated for a total heat flux of 10 kW, which is the minimum operating conditions for an IHF electrode (400 A at 25 V). The peak temperatures, presented in Table 2, are approximately 10% lower at 10 kW than at 20 kW. All eight cases are survivable. Therefore, we conclude that under normal IHF operating conditions, the smoothly rotating arc foot is safe unless the peak heat flux exceeds 300 kW/cm^2 and the rotation rate is in the low end of the postulated range.

The maximum electrode temperature does not necessarily increase with total heat flux (i.e., current), because the temperature depends on the variation of both arc-foot radius (or peak heating) and rotation rate. Winovich[5] measured a rotational frequency of 210 Hz at the minimum operating current. In general, the rotation rate should increase with electrode current[3,10] owing to the increased magnetic field; however, for a high-pressure arc, Painter[8] reports no increase in rotation rate and some arc destabilization above a certain current value. There is no good theory to predict the precise variation of peak heating and arc-foot radius with arc current. The peak heating will increase with current unless the arc-foot radius increases faster than the square root of current. The temperature may not increase with peak heating if the rotation rate also increases.

Nondimensional results from Eq. (10) for the smoothly rotating arc foot were obtained for wide parametric variation of R_s/R and $\delta^2\omega/\alpha$. Table 3 presents Φ_{max} for $\delta/R = 0.02$ and for a parameter space that represents a plausible range of operating conditions. In this parameter space, Φ_{max} is almost directly proportional to δ with a maximum deviation of 1.2% for $0.01 \leq \delta/R \leq 0.05$. Except for low frequencies and small spot sizes, the temperature is close to the value obtained from the one-dimensional approximation (derived in the Appendix)

$$\frac{R_s \Phi_{max}}{\delta} = \sum_{m=0}^{\infty} \left[\frac{\pi\alpha}{\delta^2 \lambda_{0m}}\right] \left(\frac{1 - e^{-\lambda_{0m} R_s/\pi f R}}{1 - e^{-\lambda_{0m}/f}}\right) \qquad (22)$$

where $\lambda_{0m} = \lambda_{n=0,m}$ from Eq. (15). The right side is a function of R_s/R and $\delta^2\omega/\alpha$.

Next we consider the jumping arc-foot case and in Fig. 4 present results for the heated-surface temperature [from Eq. (21)]. The arc foot is located at $\theta = 0$, but is about to jump to the next location. The total heat flux of 10 kW and peak heating of 75 W/cm^2 represent minimal operating conditions for an IHF electrode. Consider the case $N = 2$ (the solid line). The two sticking locations are situated at opposite sides of the electrode, the peak temperature reaches 2617 K at the heated spot, and the (currently) nonheated spot has cooled to about 2100 K. These values far exceed the maximum temperature of 528 K that is obtained if the arc foot is smoothly rotating (cf. Table 2), and clearly indicate a nonsurvivable operating condition where a significant thickness of electrode wall would melt.

Figure 4 also shows that as the number of sticking locations is increased, the peak temperature decreases. For $N = 5$ the peak temperature of 1450 K is marginally survivable, because the temperature cools to about 1000 K when the arc foot jumps to other locations. The case $N = 8$ is safe. Note that in Fig. 4 the individual sticking points are thermally isolated from each other. Therefore, to calculate the peak temperature, we need to consider only the $j = 0$ terms in Eq. (21) for $NR_s << R$.

To show the effect of variations in rotation rate and total heating, the dimensional calculations were repeated for $f = 100$ Hz and for total heat flux of 20 kW and peak heating of 75 kW/cm^2. The peak temperatures, presented in Table 4, increase 4–10% for the maximum heating conditions of 20 kW, and increase up to 25% for $f = 100$ Hz. The cases $N = 2$ and $N = 3$ are catastrophic. The cases $N = 5$ at $f = 500$ Hz, and $N = 8$ at $f = 100$ Hz might be survivable, and the cases $N = 8$ at $f = 500$ Hz are safe.

Results for peak heating $Q = 300$ kW/cm^2 are not presented herein, because the temperatures were too high. The maximum temperature was above 2800 and 3700 K for $N = 8$ and 5, respectively, at 10 kW total heating and $f = 500$ Hz.

Based on the dimensional calculations discussed above, we conclude that under the nominal IHF operating conditions, the jumping arc foot is not survivable unless the peak heating is lower than 100 kW/cm^2 and the number of sticking points is fortuitously large, say $N > 5$.

The maximum dimensionless temperature for $\delta/R = 0.02$ and for parametric variation of N, R_s/R, and $\delta^2\omega/\alpha$ is presented in Tables 5–8. Data for other values of δ/R are tabulated in Ref. 11. The results begin to scale proportionally with δ if $R_s > 2\delta$. For these large spot sizes, the temperature

Table 5 Φ_{max} for jumping arc foot with $N = 2$ and $\delta/R = 0.02$

$\delta^2\omega$	R_s/R values					
α	0.005	0.010	0.022	0.050	0.100	0.220
5	2.447	1.796	1.093	0.533	0.269	0.122
7	2.365	1.717	1.026	0.496	0.250	0.114
10	2.272	1.628	0.956	0.461	0.233	0.106
15	2.168	1.533	0.889	0.431	0.218	0.099
22	2.075	1.451	0.838	0.409	0.207	0.094
33	1.982	1.372	0.794	0.391	0.198	0.090
50	1.888	1.300	0.759	0.375	0.190	0.086
70	1.816	1.248	0.735	0.365	0.185	0.084
100	1.744	1.201	0.714	0.355	0.180	0.082
200	1.621	1.130	0.682	0.341	0.173	0.079

Table 6 Φ_{max} for jumping arc foot with $N = 3$ and $\delta/R = 0.02$

$\delta^2\omega$	R_s/R values					
α	0.005	0.010	0.022	0.050	0.100	0.220
5	2.301	1.655	0.971	0.459	0.231	0.105
7	2.182	1.541	0.880	0.413	0.208	0.095
10	2.056	1.425	0.796	0.374	0.189	0.086
15	1.922	1.305	0.719	0.342	0.173	0.079
22	1.803	1.204	0.662	0.318	0.161	0.073
33	1.681	1.108	0.614	0.297	0.151	0.068
50	1.561	1.021	0.574	0.280	0.142	0.064
70	1.470	0.961	0.547	0.268	0.136	0.062
100	1.381	0.907	0.524	0.258	0.131	0.059
200	1.232	0.827	0.488	0.242	0.123	0.056

Table 7 Φ_{max} for jumping arc foot with $N = 5$ and $\delta/R = 0.02$

$\delta^2\omega$	R_s/R values					
α	0.005	0.010	0.022	0.050	0.100	0.220
5	2.071	1.435	0.793	0.362	0.182	0.083
7	1.928	1.303	0.698	0.319	0.161	0.073
10	1.784	1.176	0.616	0.284	0.143	0.065
15	1.631	1.046	0.543	0.254	0.128	0.058
22	1.493	0.937	0.489	0.232	0.117	0.053
33	1.354	0.836	0.443	0.212	0.107	0.049
50	1.220	0.749	0.405	0.195	0.098	0.045
70	1.121	0.690	0.380	0.184	0.093	0.042
100	1.025	0.638	0.357	0.174	0.088	0.040
200	0.873	0.562	0.323	0.159	0.080	0.037

Table 8 Φ_{max} for jumping arc foot with $N = 8$ and $\delta/R = 0.02$

$\delta^2\omega$	R_s/R values					
α	0.005	0.010	0.022	0.050	0.100	0.220
5	1.842	1.224	0.638	0.286	0.144	0.065
7	1.694	1.092	0.554	0.250	0.126	0.057
10	1.544	0.966	0.482	0.220	0.111	0.050
15	1.384	0.839	0.418	0.194	0.098	0.044
22	1.240	0.735	0.371	0.173	0.087	0.040
33	1.098	0.642	0.330	0.156	0.078	0.036
50	0.964	0.563	0.296	0.141	0.071	0.032
70	0.868	0.511	0.273	0.131	0.066	0.030
100	0.777	0.465	0.253	0.122	0.061	0.028
200	0.638	0.397	0.223	0.108	0.055	0.025

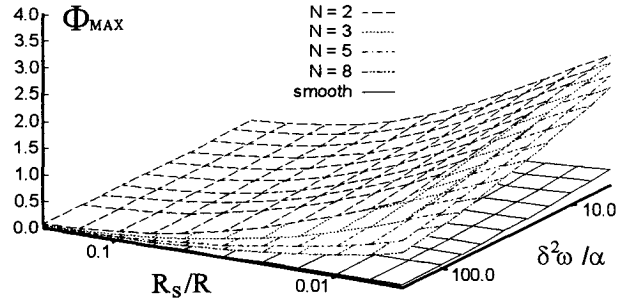

Fig. 5 Surface plot of Φ_{max} for smoothly rotating arc foot and jumping arc foot. $\delta/R = 0.02$.

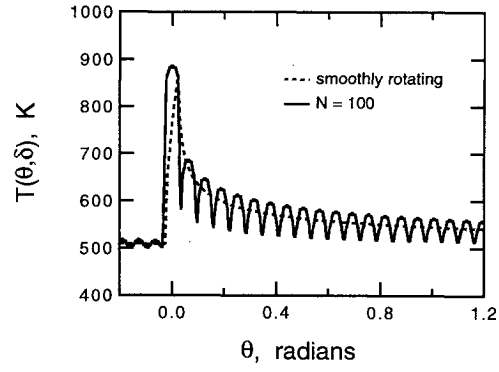

Fig. 6 Electrode surface temperature for smoothly rotating and jumping arc foot. $R = 6$ cm, $\delta = 0.254$ cm, $f = 500$ Hz, $Q = 300$ kW/cm^2, and $\pi R_s^2 Q = 20$ kW.

is close to the value obtained from the one-dimensional approximation [cf. Eq. (A3)]

$$\frac{R_s\Phi_{max}}{\delta} = \sum_{m=0}^{\infty}\left[\frac{\pi\alpha}{\delta^2\lambda_{0m}}\right]\left(\frac{1 - e^{-\lambda_{0m}/Nf}}{1 - e^{-\lambda_{0m}/f}}\right) \tag{23}$$

This equation is similar to Eq. (22), except that the right side is a function of N and $\delta^2\omega/\alpha$.

The jumping arc foot, in general, produces higher temperature than the smoothly rotating arc foot. Figure 5 presents a three-dimensional surface plot of Φ_{max} for the jumping and smoothly rotating cases. The difference between the two solutions increases as R_s/R decreases and as $\delta^2\omega/\alpha$ increases. In the parameter range of interest, Φ_{max} for $N = 2$ is 2 to 27 times the value obtained for the smoothly rotating case. The smoothly rotating arc foot is, in effect, the limit for $N \to \infty$ of the jumping arc foot. Indeed, a calculation with $N = 100$ (Fig. 6) produces a temperature profile that begins to resemble the profile obtained for the smoothly rotating arc foot under the same conditions.

Discussion

The preceding results have shown that at traditional current levels, the smoothly rotating arc foot is reasonably benign to the electrode, whereas the jumping arc foot is dangerous unless the peak heat flux is low and the number of sticking points is large. In the past, electrodes at NASA Ames have been operated above 800 A with detrimental effect on electrode lifetime. This experimental result suggests that at high current either the peak heating rises above 300 kW/cm^2 for smooth rotation or the jumping arc foot occurs more frequently.

Because future arcjet designs call for higher total current than available in existing facilities, the question that arises is how to increase the arc current per electrode without adversely affecting the operational lifetime of the electrode. We can design for higher magnetic field strength, but there is no evidence that stable, high rotation rates can be maintained at high currents. Another possibility is to make the electrode wall thinner, which would obviously improve heat transfer,

because over much of parameter space Φ_{max} is approximately proportional to δ. However, a thin wall tolerates less erosion, and so the electrode lifetime may not necessarily be increased by decreasing the wall thickness.

Unless by design we can preclude the occurrence of the jumping arc foot, alternatives to magnetically driven electrodes should be considered. Several options have been proposed.[12] A fixed tungsten cathode can provide 1000–5000 A (depending on pressure), but must be shielded from oxygen, which may not be possible in the downstream region of an arcjet. A more promising alternative is to employ a very large number of small electrodes, such as rods or hoops, each designed to withstand the local thermal load from a relatively low current of about 100 A. With suitable resistance ballasting, it is possible to split a high current between many small electrodes. However, such a scheme is useful only if the small electrodes can be packed into a reasonably short axial flow length.

Conclusions

Analytic formulations were derived for the thermal analysis of an arc heater electrode with an arc foot that rotates smoothly or which jumps between preferred sticking locations. For each case the temperature distribution for a copper electrode was obtained for the plausible range of operating conditions. Detailed results were presented for specific cases of interest and for parametric variations of the electrode operating parameters.

The results show that the smoothly rotating arc foot is an extremely safe mode of operation, whereas the jumping arc foot produces excessively high electrode surface temperatures that are not greatly alleviated by increasing the rotational frequency of the arc foot. Therefore, if the jumping state of electrode operation cannot be precluded, the existing designs do not look promising for operation at higher current levels. A distribution of small fixed electrodes may be advantageous for high current operation.

Appendix: One-Dimensional Approximation

We consider a one-dimensional slab of thickness δ exposed to heat flux $q(t) = Q$ of duration τ. The transient solution is obtained rigorously by integral transform in Ref. 13 (section 2.3: Eqs. 2-64, 2-63, and 2-74). In our notation, the solution at the heated surface after one exposure is

$$T - T_c = \frac{2\alpha}{k\delta} \sum_{m=0}^{\infty} e^{-\lambda_{0m} t} \int_0^t e^{+\lambda_{0m} t'} q(t')\, dt' = \frac{2Q\alpha}{k\delta} \sum_{m=0}^{\infty} \frac{e^{-\lambda_{0m} t}(e^{+\lambda_{0m}\tau} - 1)}{\lambda_{0m}}, \qquad \tau \le t \tag{A1}$$

where λ_{0m} is defined in Eq. (14). For repetitive heating of the slab, the temperature is obtained by summing the temperature rise owing to all previous exposures. For heating at frequency f the sum is

$$T - T_c = \frac{2Q\alpha}{k\delta} \sum_{m=0}^{\infty} \left[\frac{e^{-\lambda_{0m} t}(e^{+\lambda_{0m}\tau} - 1)}{\lambda_{0m}} \right] (1 + e^{-\lambda_{0m}/f} + e^{-2\lambda_{0m}/f} + e^{-3\lambda_{0m}/f} + \cdots) = \frac{2Q\alpha}{k\delta} \sum_{m=0}^{\infty} \frac{e^{-\lambda_{0m} t}(e^{+\lambda_{0m}\tau} - 1)}{\lambda_{0m}(1 - e^{-\lambda_{0m}/f})}, \qquad \tau \le t \le f^{-1} \tag{A2}$$

Since all terms are positive, the maximum temperature occurs at $t = \tau$. In dimensionless form the maximum temperature rise is

$$\frac{R_s \Phi_{max}}{\delta} = \sum_{m=0}^{\infty} \left(\frac{\pi\alpha}{\delta^2 \lambda_{0m}} \right) \left(\frac{1 - e^{-\lambda_{0m}\tau}}{1 - e^{-\lambda_{0m}/f}} \right) \tag{A3}$$

For the jumping arc foot $\tau = 1/Nf$ [Eq. (22)], whereas for the smoothly rotating arc foot $\tau \approx R_s/\pi f R$ [Eq. (23)], which is the time required for the arc foot to pass a given location.

References

[1]Shepard, C. E., Watson, V. R., and Stine, H. A., "Evaluation of a Constricted-Arc Supersonic Jet," NASA TN D-2066, Jan. 1964.

[2]Shepard, C. E., Ketner, D. M., and Vorreiter, J. W., "A High-Enthalpy Plasma Generator for Entry Heating Simulation," NASA TN D-4583, May 1968.

[3]Winovich, W., and Carlson, W. C. A., "The 60-MW Shuttle Interaction Heating Facility," *Proceedings of the 25th International Instrumentation Symposium*, Instrument Society of America, Pittsburgh, PA, 1979, pp. 59–75.

[4]Winovich, W., Balboni, J., and Balakrishnan, A., "Application of Numerical Simulation to Enhance Arcjet Performance Simulation," *Thermophysical Aspects of Re-Entry Flows*, edited by J. N. Moss and C. D. Scott, Vol. 103, Progress in Astronautics and Aeronautics, AIAA, New York, 1986, pp. 393–415.

[5]Winovich, W., "An Instrumentation System to Measure Arc Rotation Frequency," Ames Research Center, FluiDyne Engineering Corp., NASA Rept., Mountain View, CA, Nov. 1990.

[6]Painter, J. H., "Arc Control Experiments Using a High Performance Arc Heater," McDonnell Douglas Astronautics Co., AEDC-TR-81-20, St. Louis, MO, June 1981.

[7]Painter, J. H., "HIPERARC—A High Performance Arc Heater," AIAA Paper 83-1560, June 1983.

[8]Painter, J. H., "Arc Heater Improvement Study," McDonnell Douglas Astronautics Co., AEDC-TR-85-41, St. Louis, MO, Nov. 1984.

[9]Milos, F. S., "Flowfield Analysis for High-Enthalpy Arc Heaters," *Journal of Thermophysics and Heat Transfer*, Vol. 6, No. 3, 1992, pp. 565–568.

[10]Durgapal, P., "Current Distribution in the Cathode Area of an Arc Jet," AIAA Paper 91-1385, June 1991.

[11]Milos, F. S., and Shepard, C. E., "Thermal Analysis of an Arc Heater Electrode with a Rotating Arc Foot," AIAA Paper 93-2855, July 1993.

[12]Shepard, C. E., private communication, Oct. 1992 and Feb. 1993.

[13]Özişik, M. N., *Boundary Value Problems of Heat Conduction*, Dover, New York, 1989, pp. 59–69.